Original

Optical constants characterization of $As_{30}Se_{70-x}Sn_x$ thin films using neural networks

Attia A. Attia [a,*], Mohammed S. El-Bana [b,d], Doaa M. Habashy [c], Suzan S. Fouad [b], Mahmoud Y. El-Bakry [c]

[a] *Thin Films Laboratory, Department of Physics, Faculty of Education, Ain Shams University, Cairo, Egypt*
[b] *Nano-Science & Semiconductor Laboratories, Department of Physics, Faculty of Education, Ain Shams University, Cairo, Egypt*
[c] *Theoretical Group, Department of Physics, Faculty of Education, Ain Shams University, Cairo, Egypt*
[d] *College of Science and Art at Rass-Qassim University, PO Box 53 Postcode 51921, Saudi Arabia*

Abstract

This paper uses an artificial neural network (ANN) and resilient back-propagation (Rprop) training algorithm to determine the optical constants of $As_{30}Se_{70-x}Sn_x$ ($0 \leq x \leq 3$) thin films. The simulated values of the ANN are in good agreement with the experimental data. The ANN models performance was also examined to predict the simulated values for $As_{30}Se_{67}Sn_3$ which was not included in the training and was found to be in accordance with the experimental data. The high precision of the ANN models as well as a great guessing performance have been exhibited. Moreover, the energy gap E_g of $As_{30}Se_{70-x}Sn_x$ ($0 \leq x \leq 9$) thin films were calculated theoretically.

© 2017 Universidad Nacional Autónoma de México, Centro de Ciencias Aplicadas y Desarrollo Tecnológico. This is an open access article under the CC BY-NC-ND license (http://creativecommons.org/licenses/by-nc-nd/4.0/).

Keywords: ANN model; Optical constants; Energy gap

1. Introduction

The past few decades have seen rapid advances in the study of chalcogenide materials owing to their adequate amorphous semiconducting features (Singh, 2012). Several researchers have studied these materials as they have a wide range of unique thermal, electronic and optical properties (Aggarwal & Sanghera, 2002; Fayek, Fouad, Balboul, & El-Bana, 2007; Fouad, El-Shazly, Balboul, Fayek, & El-Bana, 2006; Fouad, El-Bana, Sharma, & Sharma, 2015; Laine & Seddon, 1995; Owen, Firth, & Ewen, 1985; Saiter, Hamou, & Vautier, 1994; Seddon, 1995; Singh, 2012). Optical properties of chalcogenide glasses have attracted significant attention due to their remarkable applications in optoelectronics and many other technological fields, particularly, in the area of thin films (Andriesh & Iovu, 2006; El-Bana, Bohdan, & Fouad, 2016; Iovu et al., 2007).

The optical properties of arsenic selenide glassy system are greatly influenced by the effect of changing its chemical composition. Adding tin to As_2Se_3 has considerable changes in both the transmission spectra and the refractive index (Fouad et al., 2006). The optical parameters for the studied As–Se–Sn amorphous system have been estimated earlier (Fouad et al., 2006) using the well-known Swanepoel method (Swanepoel, 1984) and the Wemple–DiDomenico model (Wemple, 1973; Wemple & DiDomenico, 1971). The optical band gaps for the studied compositions are also determined using the non-direct transition model proposed by Tauc's extrapolation method (Tauc, Grigorovici, & Vancu, 1966). The obtained parameters gave a clear idea about the changes in bonding arrangement due to tin addition, which affects the optical behavior of the As_2Se_3 amorphous system (Fouad et al., 2006).

The artificial neural network as program embedded in MATLAB software has been used to simulate our data. Artificial neural networks (ANNs) are biologically inspired computer programs intended to emulate the way in which the human brain processing information. These programs are mainly used in areas involving pattern mapping and pattern classification

---

* Corresponding author.
E-mail address: attia05@yahoo.com (A.A. Attia).

Peer Review under the responsibility of Universidad Nacional Autónoma de México.

such as visual images and speech recognition, especially they solve lots of problems that may arise in other conventional techniques. Recently, a great deal of attention has been paid to use such fascinating networks in solving many problems that encounter physicists due to lack of facilities. Developments in ANNs and their applications to physics have made it feasible to model numerous relations in different areas in physics (Attia, El-Nahass, El-Bakry, & Habashy, 2013; Bourouis, Meddour, & Moussaoui, 2006; Darwish et al., 2015; El-Bakry, 2003, 2004; El-Metwally, Haweel, & El-Bakry, 2000; Haweel, El-Bakry, & El-Metwally, 2003). The ANNs architecture is inspired by the structure of the human brain, which is not quite the same as the PCs utilized today (Tabet & McGahan, 2000).

In the present work, the artificial neural networks and the resilient backpropagation (Rprop) algorithm are combined to estimate the refractive index $n(\lambda)$ and the absorption index $k(\lambda)$ as a function of $As_{30}Se_{70-x}Sn_x$ thin films composition (value of x). Prediction of the simulated values of $n(\lambda)$ and $k(\lambda)$ for composition ($x = 3$) that not included in the network training was also achieved. Moreover, the artificial neural networks have enabled us to get one numerical equation which depict the spectral behavior of both $n(\lambda)$ and $k(\lambda)$. Besides, the energy gap E_g of $As_{30}Se_{70-x}Sn_x$ ($0 \leq x \leq 9$) thin films were calculated theoretically.

2. Experimental details

The amorphous nature of $As_{30}Se_{70-x}Sn_x$ ($0 \leq x \leq 3$) compositions as well as their thin films were verified firstly by X-ray diffraction (XRD) technique, type (Pw1710) (Balboul, Fouad, Fayek, & El-Bana, 2008). The choice of these three compositions renders to the fact that adding Sn to $As_{30}Se_{70}$ with a percent more than 3.5% would affect the amorphous nature of the studied compositions. Therefore, in the experimental part we have varied Sn till 3%. Thin films of our amorphous alloy of thicknesses about 500 nm were deposited on cleaned glass substrates by thermal evaporation technique at ($\sim 10^{-4}$ Pa) base pressure. The film thickness was controlled by the thickness monitor and was confirmed by using the Fizeau interferometric technique. This technique uses an optical arrangement together with interferometric principle (Fouad et al., 2006). Moreover, interference pattern have been observed in the transmittance spectra which confirms that the surface of the film is of good optical quality and the film thickness is homogeneous. Morphology and composition analysis of the alloys and their thin films were checked using scanning electron microscope (SEM) and energy dispersive spectrometry (EDS) respectively. The optical transmittances of our thin films were measured at room temperature using a double beam UV–vis–NIR spectrophotometer in the wavelength range (200–1100 nm). The optical constants $n(\lambda)$ and $k(\lambda)$ of our films have been determined using Swanepole technique (Swanepoel, 1984). Our earlier work (El-Bana & Fouad, 2017; El-Bana et al., 2016; Sharma, El-Bana, Fouad, & Sharma, 2016) and various other researchers (Márquez, González-Leal, Jiménez-Garay, Lukic, & Petrovic, 1997; Sharma, Sharda, Sharma, & Sharma, 2014) have used this technique to estimate the optical parameters for chalcogenide glasses. The determined values of n and k for

all films were found to lie within the range of the experimental error $\pm 2\%$ for n and $\pm 5\%$ for k (Fouad et al., 2006).

3. Artificial neural networks ANNs

The architecture of neural network has a number of layers (input, output, and hidden layers) that involve a number of nodes (neurons) cf., Fig. 1. These nodes in different layers are connected to each other through links named as weights. The artificial neurons are the processing units of the network as can be seen in Fig. 2.

Basically, training is considered as the main operating phase of the neural network. The training of networks includes adjusting weights and bias until the performance of networks becomes adequate. Resilient back-propagation algorithm (Rprop) is considered as one of the fastest training for artificial neural networks. The importance of (Rprop) is to eliminate the harmful effects of the magnitudes of the partial derivatives caused by the *logsig* transfer functions (the sigmoid functions) when applied to the output (a) shown in Fig. 2. The partial derivative refers to the derivative of the performance function with respect to the weights. The sign of the derivative is the factor used in determining the direction of the weight update not the magnitude of the derivative itself. A separate update value is used in determining the size of the weight change. When the derivative of the performance function with respect to that weight has the same sign for two successive iterations, an increase by a factor in the update value for each weight and bias is obtained. Whereas, a decrease by a factor in the update value is obtained, whenever the derivative with respect to weight changes sign from the previous iteration. Furthermore, the update value remains the
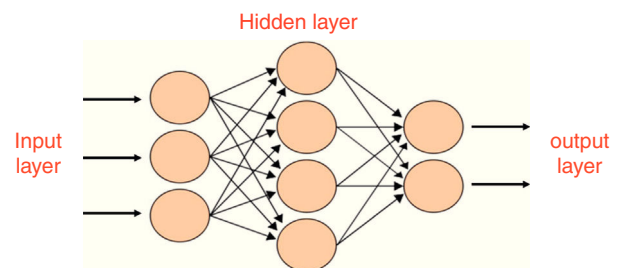

Fig. 1. Typical pattern of ANNs, with an architecture of multilayer feedforward network with one hidden layer of four neurons.
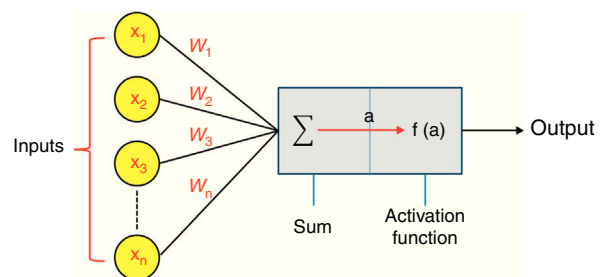

Fig. 2. Simple neuron model: each input X_n is weighted by a factor W_n. The sum of all inputs is calculated $\left(\sum_{\text{all inputs}} W_n X_n\right)$; then an activation function f is applied to the resultant a. The neural output is taken to be $f(a)$; and $f(a) =$ activation function $\left(\left(\sum_{\text{all inputs}} W_n X_n\right)\right)$.
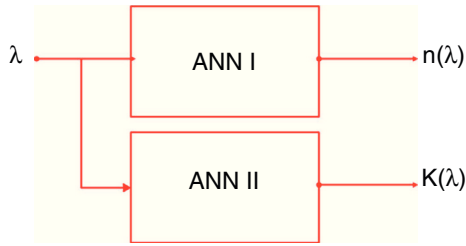
Fig. 3. Block diagram presents the proposed ANN models.

same when the derivative equals zero. Whenever the weights are oscillating the weight change will be reduced. If the weight continues to change in the same direction for several iterations, then the magnitude of the weight change will be increased (Kişi & Uncuoğlu, 2005). For a deeper understanding of the resilient backpropagation algorithm see (Riedmiller & Braun, 1994).

3.1. Modeling the optical constants using ANN model

A neural network is a powerful computational model that able to simulate and predict complex input/output relationships. In this technique, we attempted to mathematically model the optical constants $n(\lambda)$ and $k(\lambda)$ using ANNs. In this regard, two different ANN models (ANN I and ANN II) are designed to achieve this goal. A simplification of the proposed ANN models is presented in Fig. 3.

The first model (ANN I) calculates and predicts the values of refractive index, n, as a function of wavelength, λ. Whereas, the second model ANN II calculates and predicts the values of extinction coefficient, k, as a function of wavelength λ. The ANN I model has five hidden layers of 260, 210, 180, 200 and
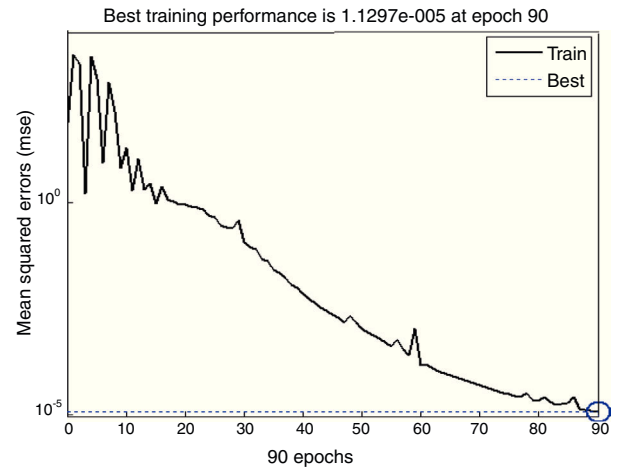

Fig. 4. Performance of ANN for modeling refractive index n of $As_{30}Se_{70-x}Sn_x$ thin films.

220 neurons, while the second model (ANN II) has five hidden layers of 20, 10, 10, 15 and 25 neurons. The transfer functions of these hidden layers were chosen to be *logsig*, while the output to be *pureline* as explained in Appendix A.

4. Results and discussion

Neural networks were trained simultaneously using experimental data of refractive index $n(\lambda)$ of $As_{30}Se_{70-x}Sn_x$ thin films for three different compositions ($x = 0, 1, 2$) (Fouad et al., 2006). Fig. 4 shows the training procedure which reveals that the mean squared error of the network starting at a large value and diminishing to reach a best value of 1.1297×10^{-5} after
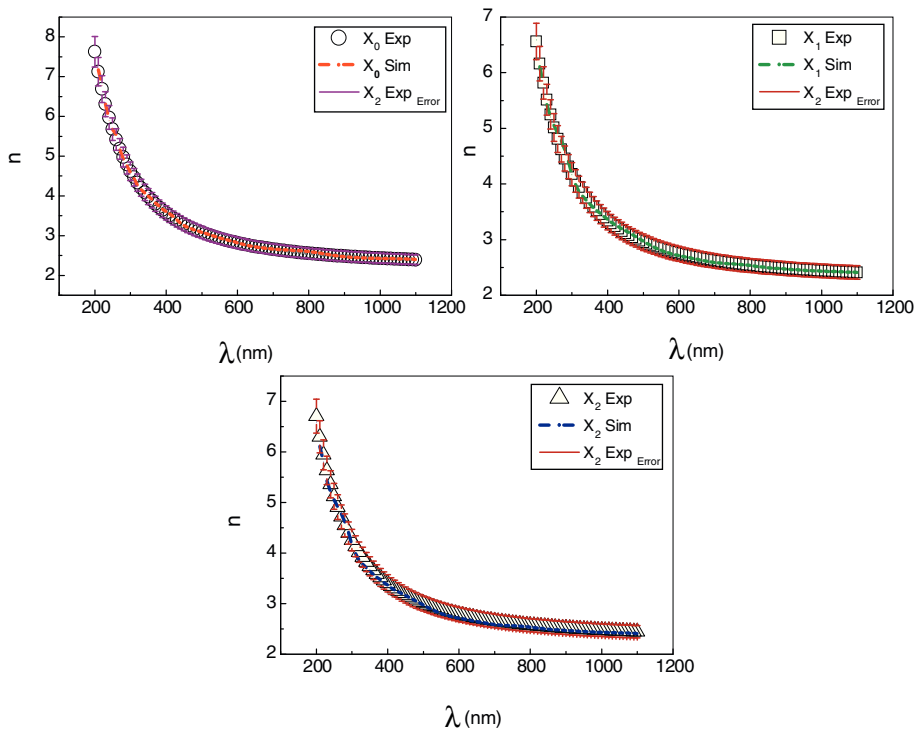

Fig. 5. Experimental data and simulation results from ANN model for refractive index $n(\lambda)$ of $As_{30}Se_{70-x}Sn_x$ thin films for different compositions ($x = 0, 1, 2$).
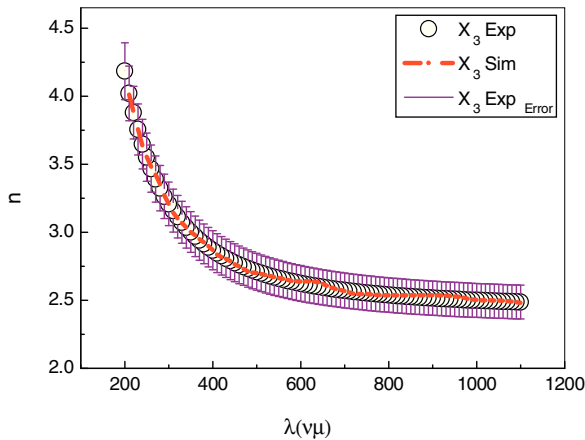
Fig. 6. The predicted refractive index $n(\lambda)$ by ANN model altogether with the experimental data of $As_{30}Se_{67}Sn_3$ thin film which is not included in the network training.

Fig. 7. Performance of ANN for modeling absorption index k of $As_{30}Se_{70-x}Sn_x$ thin films.

90 epochs; where epochs means the number of training. Reaching this stage confirms that the network has been learnt. The obtained equation that represents the refractive index n is given in Appendix A.

The simulation results of refractive index $n(\lambda)$ of $As_{30}Se_{70-x}Sn_x$ ($x = 0, 1, 2$) thin films together with the corresponding experimental data are depicted in Fig. 5. It is clearly observed that the measured curves and the curves achieved by ANN are in good agreement. This denotes that the trained network adopt optimal generalization performance. The dispersion curve of refractive index n shows normal dispersion at $\lambda > 700$ nm with value of ($n = 2.396$) at ($\lambda = 1000$ nm) for composition ($x = 0$). The n value was found to increase with increasing value of x at the same wavelength λ can be seen in both Fig. 5 and Table 1.

The refractive index $n(\lambda)$ of $As_{30}Se_{67}Sn_3$ film was predicted using the ANN I model and was represented together with the corresponding experimental data in Fig. 6. This composition was not included in the neural network training for modeling the refractive indices. Comparing curves shown in Fig. 6 demonstrates that the measured curve and the curve computed by ANN I are almost superimposed. In the same trend, the n value of ($n = 2.488$) was found to increase with increasing value of x at ($\lambda = 1100$ nm) which gives a good impression of the network performance.

Neural network modeling for absorption index $k(\lambda)$ was also achieved to complete determination of the optical constants of $As_{30}Se_{70-x}Sn_x$ thin films. We followed the same approach that has been applied in case of modeling the refractive indices. Neural networks were trained simultaneously using experimental data of absorption index $k(\lambda)$ of $As_{30}Se_{70-x}Sn_x$ thin films for three different compositions ($x = 0, 1, 2$). Fig. 7 presents the network performance, which reveals that the mean squared error of the network begun at a large value and decreased reaching to a best value of about 2.06×10^{-5} at 700 epochs. Again, these results have confirmed that the network has been learnt. In addition, the obtained equation that represents the extinction coefficient k is given in Appendix A which is the same for the refractive index n. This consistency obeys the approach of Kramers–Kronig (KK) model.

The simulation results of absorption index $k(\lambda)$ of $As_{30}Se_{70-x}Sn_x$ thin films together with the corresponding experimental data are represented in Fig. 8. The obtained curves reveal that the results of absorption indices based on ANN II are in good agreement with their corresponding experimental data. The absorption index k decreases as a function of wavelength λ and reaches to zero value at about 700 nm for a composition of ($x = 0$). This cutoff value of k decreases with increasing the value of x in the composition.

Another testing was carried out to confirm the validity of our network performance, which is the prediction of absorption

Table 1
Optical refractive indices n and energy gap E_g of $As_{30}Se_{70-x}Sn_x$ thin films for different compositions.

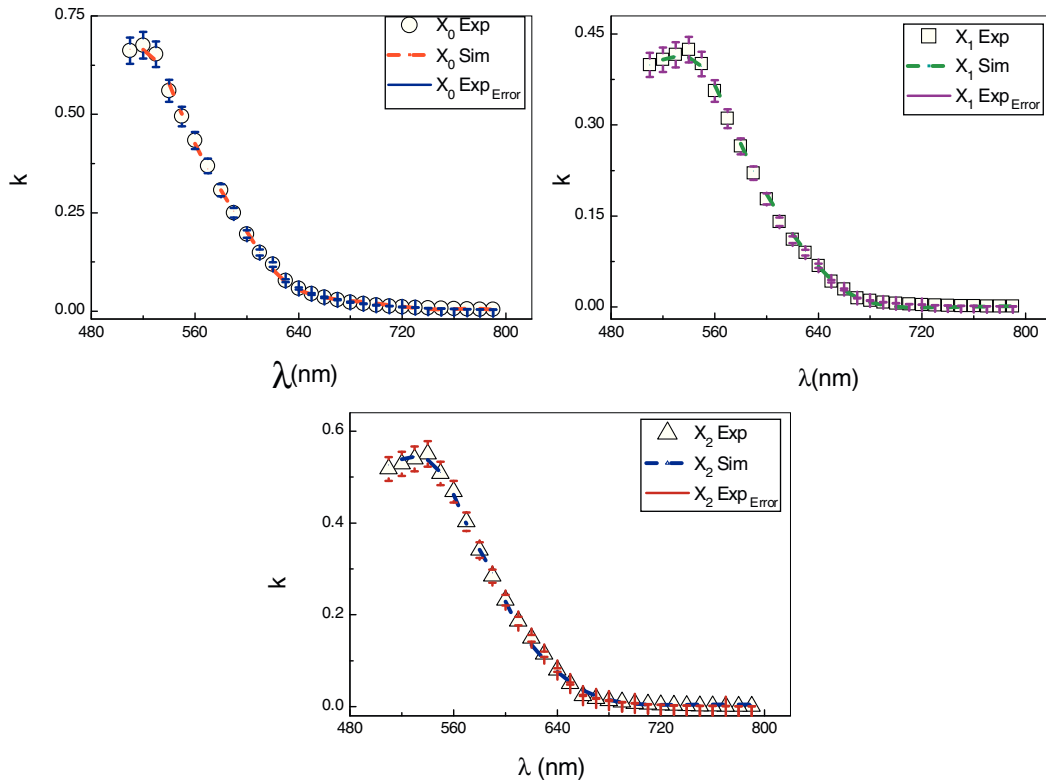| Compositions	$E_g^{th}(eV)$	$E_g^{exp}(eV)$	n_{exp} at $\lambda = 1100$ nm	n_{sim} [21]
$As_{30}Se_{70}$	1.767	1.81 ± 0.03	2.396	2.8471
$As_{30}Se_{69}Sn_1$	1.7477	1.78 ± 0.03	2.409	2.8686
$As_{30}Se_{68}Sn_2$	1.7284	1.77 ± 0.03	2.444	2.8891
$As_{30}Se_{67}Sn_3$	1.7091	1.76 ± 0.03	2.488	2.9109
$As_{30}Se_{66}Sn_4$	1.6898	–	–	2.9327
$As_{30}Se_{65}Sn_5$	1.6705	–	–	2.9544
$As_{30}Se_{64}Sn_6$	1.6512	–	–	2.9757
$As_{30}Se_{63}Sn_7$	1.6319	–	–	2.9965
$As_{30}Se_{62}Sn_8$	1.6126	–	–	3.0167
$As_{30}Se_{61}Sn_9$	1.5933	–	–	3.0360

Fig. 8. The obtained results from ANN model for absorption indices $k(\lambda)$ compared to experimental data of $As_{30}Se_{70-x}Sn_x$ thin films for different compositions ($x = 0, 1, 2$).

index $k(\lambda)$ of $As_{30}Se_{70-x}Sn_x$ thin films for composition ($x = 3$). The one that was not included in the neural network training for modeling the absorption indices. Fig. 9 presents the predicted results of $k(\lambda)$ for composition ($x = 3$) which generated from ANN model in addition to the corresponding experimental data. A slight difference between the measured and predicted values, especially at wavelength <600 nm with maintaining the same behavior has been observed.

The observed decrease in the refractive index, n, and the extinction coefficient, k, with the increase in wavelength may be correlated with the increase in the transmittance and decrease in the absorption coefficient. Building on obtained results, it is easy to get the dispersion parameters and energy gaps for
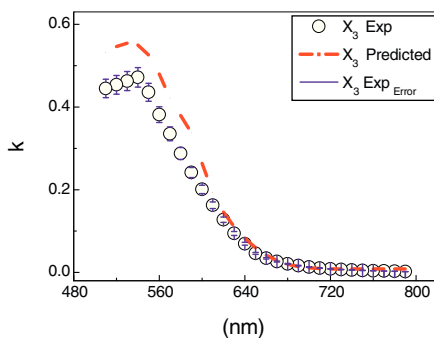

Fig. 9. Prediction of absorption index $k(\lambda)$ by ANN model and experimental data of $As_{30}Se_{70-x}Sn_x$ thin films for composition ($x = 3$) which is not included in the network training.

different compositions of $As_{30}Se_{70-x}Sn_x$ thin films using the simulation results of $n(\lambda)$ and $k(\lambda)$ respectively. The simulation results of $n(\lambda)$ and $k(\lambda)$ generated from ANN model showed almost exact fitting to the corresponding experimental data, which is not available through the other conventional theoretical techniques. This gives the ANN the facilities of wide usage in modeling of numerous relations in different areas in physics.

To overcome the unavailability of compositions ($4 \leq x \leq 9$) of $As_{30}Se_{70-x}Sn_x$ thin films, energy gaps were calculated theoretically for compositions ($0 \leq x \leq 9$) and tabulated in Table 1. The band gap for the compositions under investigations has also been calculated theoretically using the formula (Sharma, Tripathi, & Barman, 2008)

$$E_g^{th}(\text{As–Se–Sn}) = aE_g(\text{As}) + bE_g(\text{Se}) + cE_g(\text{Sn}) \qquad (1)$$

where a, b, and c are the elements volume fractions, and $E_g(\text{As}) = 1.2$ eV, $E_g(\text{Se}) = 2.01$ eV, and $E_g(\text{Sn}) = 0.08$ eV (Strehlow & Cook, 1973) are the optical gaps of elements.

For comparison, the measured energy gaps through absorption data were also included in Table 1. Furthermore, the experimental data of n_{exp}, and the simulated ones n_{sim} generated from both the present work and study performed by Attia et al. (2013) of the refractive indices of $As_{30}Se_{70-x}Sn_x$ thin films were also included in Table 1. The values of n_{sim} shown in the fourth column of Table 1 were predicted using method based on ANN which is described (Attia et al., 2013) for energy gap values given in the second column. These predicted values of n are in visible light at normal dispersion.

5. Conclusion

The following conclusions can be drawn from the present analysis that used an artificial neural network (ANN) to understand the effect of Sn addition on the optical constants characterization of $As_{30}Se_{70-x}Sn_x$ $(0 \leq x \leq 3)$ thin films:

- Both experimental and simulated values are found to be in good agreement.
- The physical interpretation of the ANN model performance for predicting the simulated values of $n(\lambda)$ and $k(\lambda)$ for $As_{30}Se_{67}Sn_3$ thin film is in accordance with the experimental data.
- It is clear from the calculated results that the high precision of ANN model gives a great performance for optical constants and related parameters as well and gives the ANN the merits of wide usage in modeling of other relations in different areas in physics.
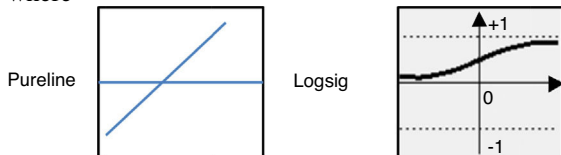
Conflict of interest

The authors have no conflicts of interest to declare.

Appendix A.

The equation which describes both $n(\lambda)$ and $k(\lambda)$ of $As_{30}Se_{70-x}Sn_x$ thin films for different compositions is given by:

n or k = pureline[net.LW{6,5}logsig(net.LW{5,4}logsig(net.LW{4,3}logsig(net.LW{3,2}logsig(net.LW{2,1}logsig(net.IW(1,1)T + net.b{1}) + net.b{2}) + net.b{3}) + net.b{4}) + net.b{5}) + net.b{6}]

where

T is the input (λ)
net.IW {1, 1} is linked weights between the input layer and first hidden layer,
net.LW {2, 1} is linked weights between first and second hidden layer.
net.LW {3, 2} is linked weights between the second and third hidden layer,
net.LW {4, 3} is linked weights between the third and fourth hidden layer,
net.LW {5, 4} is linked weights between the fourth and fifth hidden layer,
net.LW {6, 5} is linked weights between the fifth and output layer,
net.b{1} is the bias of the first hidden layer,
net.b{2} is the bias of the second hidden layer
net.b{3} is the bias of the third hidden layer,
net.b{4} is the bias of the fourth hidden layer

net.b{5} is the bias of the fifth hidden layer, and
net.b{6} is the bias of the output layer

References

Aggarwal, I. D., & Sanghera, J. S. (2002). Development and applications of chalcogenide glass optical fibers at NRL. *Journal of Optoelectronics and Advanced Materials, 4*(3), 665–678.

Andriesh, A., & Iovu, M. (2006). Optical properties of As–Se amorphous composites. *Journal of Optoelectronics and Advanced Materials, 8*, 2080–2085.

Attia, A., El-Nahass, M., El-Bakry, M., & Habashy, D. (2013). Neural networks modeling for refractive indices of semiconductors. *Optics Communications, 287*, 140–144.

Balboul, M. R., Fouad, S. S., Fayek, S. A., & El-Bana, M. S. (2008). Short-range order analysis and electrical properties of $As_{30}Se_{70-x}Sn_x$ glassy system. *Journal of Alloys and Compounds, 460*(1), 570–576.

Bourouis, C., Meddour, A., & Moussaoui, A. (2006). Determination of optical properties of $Al_{80}Mn_{20}$ quasi-crystalline alloy using neural networks. *Journal of Molecular Structure: THEOCHEM, 777*(1), 45–51.

Darwish, A. A. A., Hanafy, T. A., Attia, A. A., Habashy, D. M., El-Bakry, M. Y., & El-Nahass, M. M. (2015). Optoelectronic performance and artificial neural networks (ANNs) modeling of n-InSe/p-Si solar cell. *Superlattices and Microstructures, 83*, 299–309.

El-Bakry, M. Y. (2003). Feed forward neural networks modeling for K–P interactions. *Chaos, Solitons & Fractals, 18*(5), 995–1000.

El-Bakry, M. Y. (2004). A study of K–P interaction at high energy using adaptive fuzzy inference system interactions. *International Journal of Modern Physics C, 15*(07), 1013–1020.

El-Bana, M. S., Bohdan, R., & Fouad, S. S. (2016). Optical characteristics and holographic gratings recording on $As_{30}Se_{70}$ thin films. *Journal of Alloys and Compounds, 686*, 115–121.

El-Bana, M. S., & Fouad, S. S. (2017). Opto-electrical characterisation of $As_{33}Se_{67-x}Sn_x$ thin films. *Journal of Alloys and Compounds, 695*, 1532–1538.

El-Metwally, K. A., Haweel, T. I., & El-Bakry, M. Y. (2000). A universal neural network presentation for Hadron–Hadron interactions at high energy. *International Journal of Modern Physics C, 11*(03), 619–628.

Fayek, S. A., Fouad, S. S., Balboul, M. R., & El-Bana, M. S. (2007). Crystallization kinetics in As–Se–Sn glassy system. *Physica B: Condensed Matter, 388*(1), 230–236.

Fouad, S. S., El-Shazly, E. A. A., Balboul, M. R., Fayek, S. A., & El-Bana, M. S. (2006). Optical parameter studies of thermally evaporated As–Se–Sn glassy system. *Journal of Materials Science: Materials in Electronics, 17*(3), 193–198.

Fouad, S. S., El-Bana, M. S., Sharma, P., & Sharma, V. (2015). Analysis of chemical ordering and fragility for Ge–Se–In glasses. *Applied Physics A, 120*, 137–143.

Haweel, T. I., El-Bakry, M. Y., & El-Metwally, K. A. (2003). Hadron–hadron interactions at high energy via Rademacher functions. *Chaos, Solitons & Fractals, 18*(1), 159–168.

Iovu, M., Harea, D., Cojocaru, I., Colomeico, E., Prisacari, A., & Ciorba, V. (2007). Optical properties and photoinduced absorption in As–Se and As_2Se_3: Sn thin films. *Journal of Optoelectronics and Advanced Materials, 9*(10), 3138–3142.

Kişi, Ö., & Uncuoğlu, E. (2005). Comparison of three back-propagation training algorithms for two case studies. *Indian Journal of Engineering & Materials Sciences, 12*(5), 434–442.

Laine, M., & Seddon, A. (1995). Chalcogenide glasses for acousto-optic devices. *Journal of Non-Crystalline Solids, 184*, 30–35.

Márquez, E., González-Leal, J. M., Jiménez-Garay, R., Lukic, S. R., & Petrovic, D. M. (1997). Refractive-index dispersion and the optical-absorption edge of wedge-shaped thin films of $Cu_xAs_{50}Se_{50-x}$ metal–chalcogenide glasses. *Journal of Physics D: Applied Physics, 30*(4), 690–702.

Owen, A., Firth, A., & Ewen, P. (1985). Photo-induced structural and physico-chemical changes in amorphous chalcogenide semiconductors. *Philosophical Magazine B, 52*(3), 347–362.

Riedmiller, M., & Braun, H. (1994). *Rprop-description and implementation details. Technical report, Citeseer*.

Saiter, J., Hamou, A., & Vautier, C. (1994). Physical aging kinetics in vitreous Se-based alloys. *Journal of Non-Crystalline Solids, 172*, 580–583.

Seddon, A. (1995). Chalcogenide glasses: a review of their preparation, properties and applications. *Journal of Non-Crystalline Solids, 184*, 44–50.

Sharma, I., Tripathi, S., & Barman, P. (2008). Correlation between the physical and optical properties of the a-Ge–Se–In–Bi system. *Philosophical Magazine, 88*(25), 3081–3092.

Sharma, N., Sharda, S., Sharma, V., & Sharma, P. (2014). Linear and nonlinear optical properties of quaternary chalcogenide glasses. *Technology Letters, 1*(8), 9–11.

Sharma, P., El-Bana, M. S., Fouad, S. S., & Sharma, V. (2016). Effect of compositional dependence on physical and optical parameters of $Te_{17}Se_{83-x}Bi_x$ glassy system. *Journal of Alloys and Compounds, 667*, 204–210.

Singh, A. K. (2012). A short over view on advantage of chalcogenide glassy alloys. *Journal of Non-Oxide Glasses, 3*, 1–4.

Strehlow, W., & Cook, E. (1973). Compilation of energy band gaps in elemental and binary compound semiconductors and insulators. *Journal of Physical and Chemical Reference Data, 2*(1), 163–200.

Swanepoel, R. (1984). Determination of surface roughness and optical constants of inhomogeneous amorphous silicon films. *Journal of Physics E: Scientific Instruments, 17*(10), 896.

Tabet, M. F., & McGahan, W. A. (2000). Use of artificial neural networks to predict thickness and optical constants of thin films from reflectance data. *Thin Solid Films, 370*(1), 122–127.

Tauc, J., Grigorovici, R., & Vancu, A. (1966). Optical properties and electronic structure of amorphous germanium. *Physica Status Solidi (b), 15*(2), 627–637.

Wemple, S. (1973). Refractive-index behavior of amorphous semiconductors and glasses. *Physical Review B, 7*(8), 3767.

Wemple, S., & DiDomenico, M., Jr. (1971). Behavior of the electronic dielectric constant in covalent and ionic materials. *Physical Review B, 3*(4), 1338.